Processing and Application of Ceramics 13 [4] (2019) 323–332
https://doi.org/10.2298/PAC1904323O

The influence of the partially europium substitution on the AC electrical properties of $BiSr_2CaCu_2O_{6.5}$ ceramics

Zeynep Güven Özdemir*, Mehmet Kılıç, Yaşar Karabul, Seda Erdönmez, Orhan İçelli

Department of Physics, Faculty of Arts and Sciences, Yildiz Technical University, 34220, Davutpasa, Esenler, İstanbul, Turkey

Received 16 January 2019; Received in revised form 29 April 2019; Received in revised form 1 August 2019; Accepted 18 September 2019

Abstract

In this work, $Eu_xBi_{1-x}Sr_2CaCu_2O_{6.5}$ (where x = 0, 0.3, 0.5) samples were prepared by solid-state reaction method and sintered at 950 °C for 24 h. The structural characterizations were done by X-ray diffraction, X-ray fluorescence, scanning electron microscope and Fourier transformed infrared spectroscopy. The thermal stability of the samples was also analysed by thermogravimetric TG and DTA measurements. It was shown that $Eu_{0.5}Bi_{0.5}Sr_2CaCu_2O_{6.5}$ sample exhibited high dielectric constant and low dielectric loss relative to $BiSr_2CaCu_2O_{6.5}$ material. Thus, the dielectric loss was lowered by heavy rare earth metal substitution on Bi-Sr-Ca-Cu-O ceramics while the dielectric constant still remained high. Temperature-dependent complex electrical modulus spectra obtained between 296 and 433 K also revealed the temperature-activated relaxation process in the materials which can be attributed to the Maxwell-Wagner type polarization effect. Ultimately, it was suggested that the $Eu_{0.5}Bi_{0.5}Sr_2CaCu_2O_{6.5}$ ceramics may have a promising potential for applications which require high dielectric constant with a low dielectric loss.

Keywords: *solid state synthesis, Eu substituted $BiSr_2CaCu_2O_{6.5}$, dielectric properties, impedance spectroscopy*

I. Introduction

High-performance dielectric materials, known as high dielectric constant materials ($\varepsilon' \geq 10^3$), are expected to play increasingly important roles in the next generation of electronics and large scale integrated microelectronics technology. In recent years, a great number of studies have focused on the production of new, high quality and high-*k* gate dielectrics on semiconductors surface. Silicon dioxide (SiO_2) is the most used dielectric gate material in electronics, but the thermally grown SiO_2 has many disadvantages in microelectronics, such as thermodynamically and electrically unstable high-quality interface state density [1]. In this context, the preparation of new materials, which both extend the limits of silicon dioxide and have better electrical insulation properties, has become increasingly important.

Silicone-based ceramic materials, such as $HfSiO_4$, $ZrSiO_4$ are also commonly used interlayer dielectric materials in high-density microelectronic packaging [2,3]. Additionally, many heavy metal oxides, such as ZrO_2, HfO_2, Al_2O_3, (Ba,Sr)TiO_3, CeO_2, Y_2O_3, La_2O_3, Ta_2O_5 and TiO_2, have been proposed as promising alternatives to SiO_2 in the next generation integrated circuits. These materials are either oxides of 4*d* and 5*d* transition metals or rare earth elements [4]. From this point of view, a partially heavy rare earth element (europium) substituted Bi-based copper oxide layered materials were developed for achieving better insulating properties for microelectronic technology.

As it is known, Bi-based copper oxide layered materials have exotic properties. For example, $Bi_2Sr_2CaCu_2O_8$ and $Bi_2Sr_2Ca_2Cu_3O_{10}$ exhibit superconductivity below the critical transition temperatures of 85 K and 110 K, respectively [5]. Additionally, they are good insulating materials at room temperature. Their magnetic and electrical properties between liquid helium and room temperatures have been investigated in details by many researchers. However, the dielectric proper-

* Corresponding authors: tel: +90 212 3834293,
e-mail: *zgozdemir@gmail.com*

ties of $BiSr_2CaCu_2O_{6.5}$, belonging to the same family, have not been examined until now. In this study, we have focused on the related Bi-based copper oxide layered ceramic perovskite material and the improvement of its dielectric properties. For this purpose europium, i.e. heavy rare earth element, partially substituted $BiSr_2CaCu_2O_{6.5}$ materials have been prepared for the first time. While pure $BiSr_2CaCu_2O_{6.5}$ material has high dielectric constant and very high dielectric loss, europium substituted $BiSr_2CaCu_2O_{6.5}$ ceramics have higher dielectric constant and lower dielectric loss relative to pure $BiSr_2CaCu_2O_{6.5}$.

II. Experimental

2.1. Preparation of $Eu_xBi_{1-x}Sr_2CaCu_2O_{6.5}$ ceramics

Eu_2O_3 (99.99%), Bi_2O_3 (99.99%), SrO (99.99%), CaO (99.99%) and CuO (99.99%) powders were used as precursors and supplied from Sigma Aldrich. The pure $BiSr_2CaCu_2O_{6.5}$ was synthesized by conventional solid-state reaction method summarized in Fig. 1. The starting precursor powders (Bi_2O_3, SrO, CaO and CuO) were mixed in appropriate stoichiometric ratios which give $BiSr_2CaCu_2O_{6.5}$ and then ground in an agate mortar for 2 h. The resultant powder was pressed into a pellet under the pressure of approximately 10^9 Pa. The pellet was placed in Al_2O_3 crucible and heated at a rate of 1 °C/min to 950 °C for 24 h in an atmospheric environment. The sample was ground for 15 min to obtain fine powder mixture which was again pressed into a pellet. Finally, the pellet was sintered at 950 °C for 24 h in an atmospheric environment. Similar procedure was used for preparation of Eu substituted Bi-based materials. The Eu substituted Bi-based ceramics ($Eu_xBi_{1-x}Sr_2CaCu_2O_{6.5}$ where $x = 0.3$ and 0.5) were prepared by mixing Eu_2O_3, Bi_2O_3, SrO, CaO and CuO powders in appropriate stoichiometric ratios. The mixtures were ground in an agate mortar for 2 h and then the Eu substituted Bi-based samples were obtained by using the same process given in Fig. 1.

2.2. Characterization techniques

The Fourier-transformed infrared (FTIR) spectra of the samples were measured by NICOLET iS10 FTIR spectrometer (Thermo Fisher Scientific, USA) operated in transmission mode with the spectral region from 4000 to 500 cm^{-1}.

Chemical analyses of the pure $BiSr_2CaCu_2O_{6.5}$ and Eu substituted $BiSr_2CaCu_2O_{6.5}$ powders were determined by X-ray fluorescence (XRF) measurements performed with the equipment model X-123SDD from Amptek, which carries an Au-target X-ray tube (30 kV, 100 μA). The system consists of an X-ray tube, a sample holder and a silicon drift detector at a scattering angle of 90°. Microstructure of the samples was observed by scanning electron microscope (SEM, Zeiss-EVO® LS 10 model). Additionally, the mass densities of the samples were calculated via the Archimedes' principle by using ethyl alcohol as an immersion liquid.

The thermal stabilities of the samples were analysed by SII Nanotechnology Exstar 6000 TG/DTA6300 thermogravimetric-differential thermal analyser (TG-DTA) with programmed heating at 1 °C/min from 25 to 820 °C under the nitrogen atmosphere.

X-ray powder diffraction (XRD) pattern for each sample was obtained by Rigaku model XRD device (at 40 kV, 40 mA) using CuK_α (1.54 Å) radiation in the range $2\theta = 20–65°$ at room temperature. The XRD patterns of the samples were analysed by MDI Jade 6.5 program.

2.3. Impedance measurements

Impedance measurements were performed by NOVO Control Broadband Dielectric/Impedance analysers with Quatro Cryosystem in the frequency range between 1 Hz–40 MHz within the temperature interval of

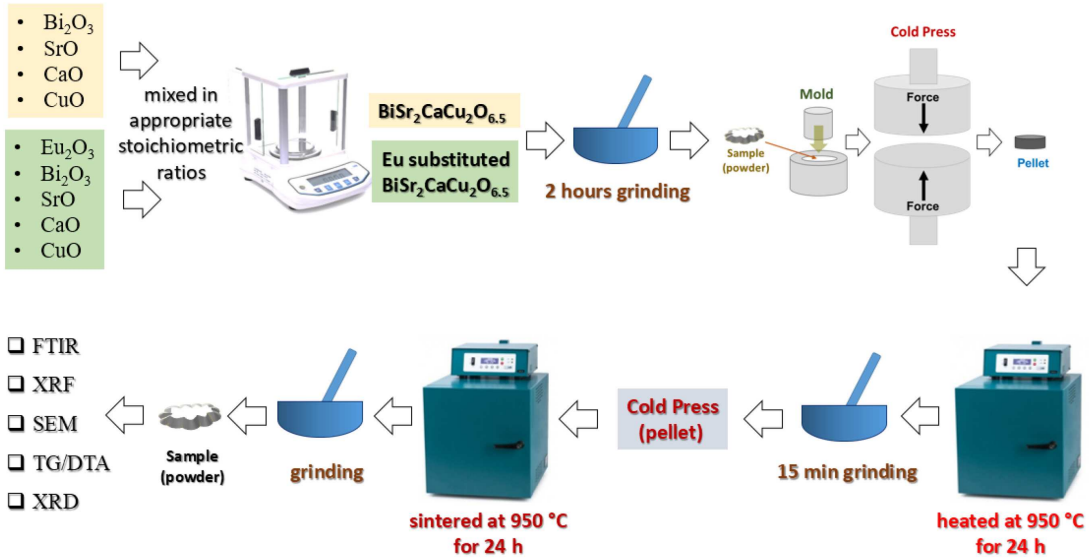

Figure 1. The samples preparation steps

296–433 K. The measurements were carried out with a two-point probe technique. The samples, prepared in the form of a pellet with 1.0 cm in diameter and 1.4–1.8 mm thickness, were placed between two gold electrodes whose surfaces totally overlap the faces of the samples. The diameter of the electrode was 2.0 cm and the active electrode area was 6.283 cm^2. The results were also transferred to a computer with GPIB data cable and simultaneously recorded by the computer.

III. Results and discussion

3.1. Structural characterization

FTIR spectra of the samples heated at 950 °C are given in Fig. 2. The band at 1444 cm^{-1} may be due to bending vibrations from O–H groups and the band at 1041 cm^{-1} can be assigned to Sr–O–Sr stretching vibrations. Therefore, the IR spectra confirmed the formation of SrO with hydroxyl groups due to the presence of surface water and did not exhibit bands corresponding to organic residues [6]. The band at 855 cm^{-1} represented Bi–O symmetrical stretching vibration in BiO_3 units [7] and 575 cm^{-1} was interpreted as vibrations of Bi–O bonds in the distorted BiO_6 polyhedra [8]. The characteristic band at 624 cm^{-1} showed the bending vibrations of the CuO crystal lattice [9]. The band observed at 586 cm^{-1} showed the presence of Ca=O group in the samples [10]. The characteristic band of Eu_2O_3 vibrations generally appears at 470 cm^{-1} [11]. Since the spectral measurement region of the spectrometer does not cover the wave numbers smaller than 500 cm^{-1}, the characteristic Eu_2O_3 vibration band has not been observed in Fig. 2. However, the presence of Eu in the material has been confirmed by XRF results (Fig. 3). On the other hand, as the Eu substitution increases, the intensity of the band related to the Bi–O symmetrical stretching vibration observed at 855 cm^{-1} decreases. Additionally, a weak shoulder at 865 cm^{-1} has been observed in the FTIR spectrum of the $Eu_{0.5}Bi_{0.5}Sr_2CaCu_3O_{6.5}$. The shoulder at the vicinity of 865 cm^{-1} is related to the vibrations of strongly distorted [BiO_6] octahedral units [12–14].

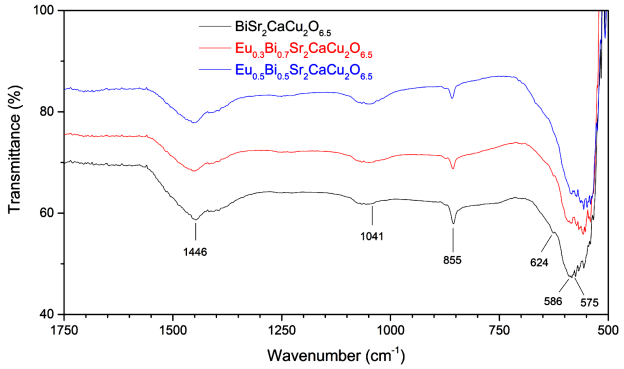

Figure 2. FTIR spectra of the powders (heated at 950 °C): a) $BiSr_2CaCu_2O_{6.5}$, b) $Eu_{0.3}Bi_{0.7}Sr_2CaCu_3O_{6.5}$ and c) $Eu_{0.5}Bi_{0.5}Sr_2CaCu_3O_{6.5}$

As shown in Fig. 3, the fluorescent peaks of Ca, Cu, Bi, and Sr were observed for $BiSr_2CaCu_2O_{6.5}$ sample between 3.692 and 15.836 keV. In addition to these fluorescent peaks, partially Eu substituted samples exhibited two peaks at 5.846 and 6.456 keV that correspond to Eu. Moreover, as the europium content in the samples increased, the height of the peaks increased. The

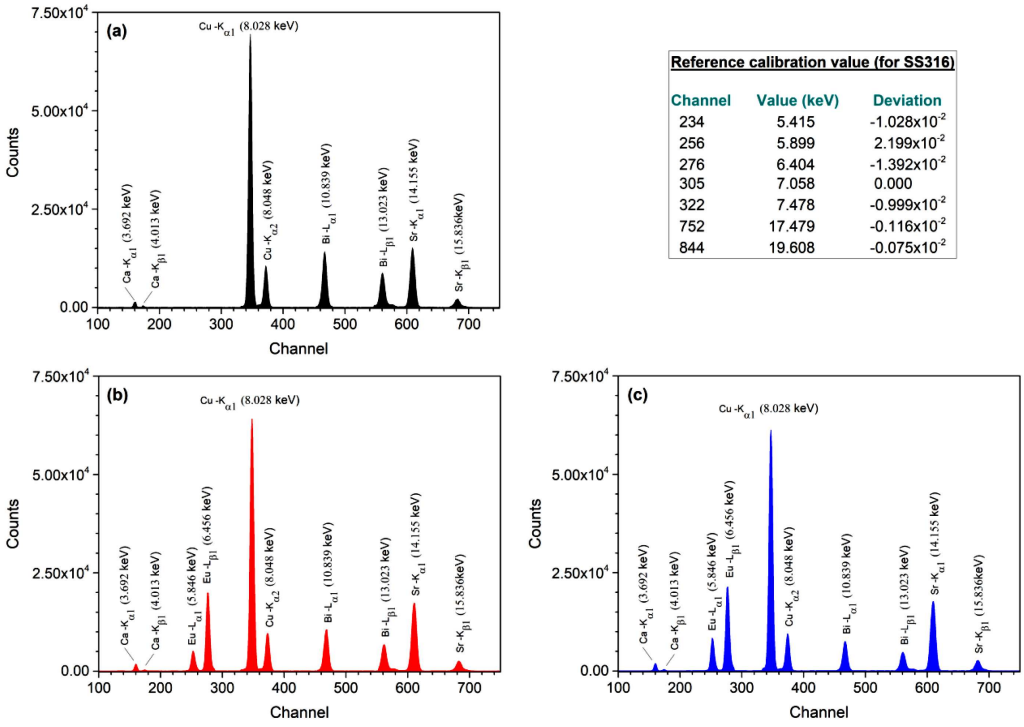

Reference calibration value (for SS316)

Channel	Value (keV)	Deviation
234	5.415	-1.028×10^{-2}
256	5.899	2.199×10^{-2}
276	6.404	-1.392×10^{-2}
305	7.058	0.000
322	7.478	-0.999×10^{-2}
752	17.479	-0.116×10^{-2}
844	19.608	-0.075×10^{-2}

Figure 3. XRF results of the powders (heated at 950 °C): a) $BiSr_2CaCu_2O_{6.5}$, b) $Eu_{0.3}Bi_{0.7}Sr_2CaCu_3O_{6.5}$ and c) $Eu_{0.5}Bi_{0.5}Sr_2CaCu_3O_{6.5}$

Table 1. Chemical composition of the samples

Sample	$BiSr_2CaCu_2O_{6.5}$	$Eu_{0.3}Bi_{0.7}Sr_2CaCu_3O_{6.5}$	$Eu_{0.5}Bi_{0.5}Sr_2CaCu_3O_{6.5}$
	Concentration [wt.%]		
Eu	0	7.14	12.12
Bi	31.89	22.92	16.67
Sr	26.74	27.46	27.95
Ca	6.12	6.28	6.39
Cu	19.39	19.91	20.27
O	15.86	16.29	16.58

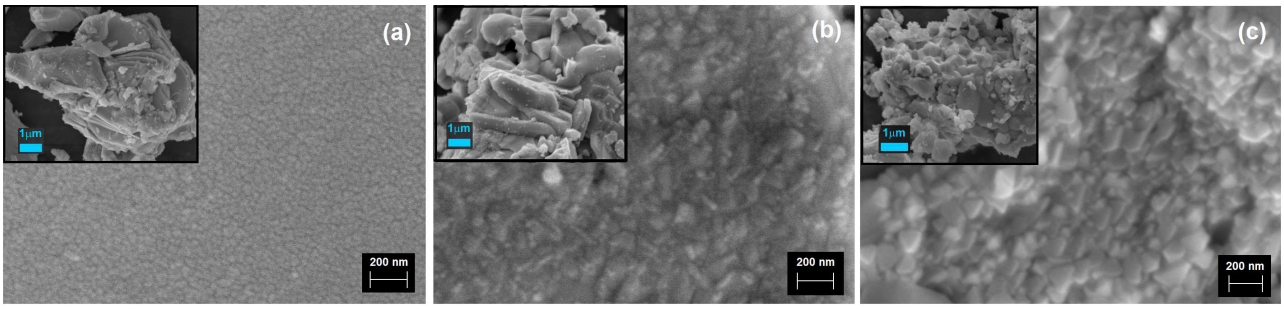

Figure 4. The SEM micrographs of the sintered samples: a) $BiSr_2CaCu_2O_{6.5}$, b) $Eu_{0.3}Bi_{0.7}Sr_2CaCu_3O_{6.5}$ and c) $Eu_{0.5}Bi_{0.5}Sr_2CaCu_3O_{6.5}$ (insets show the surface of the powders)

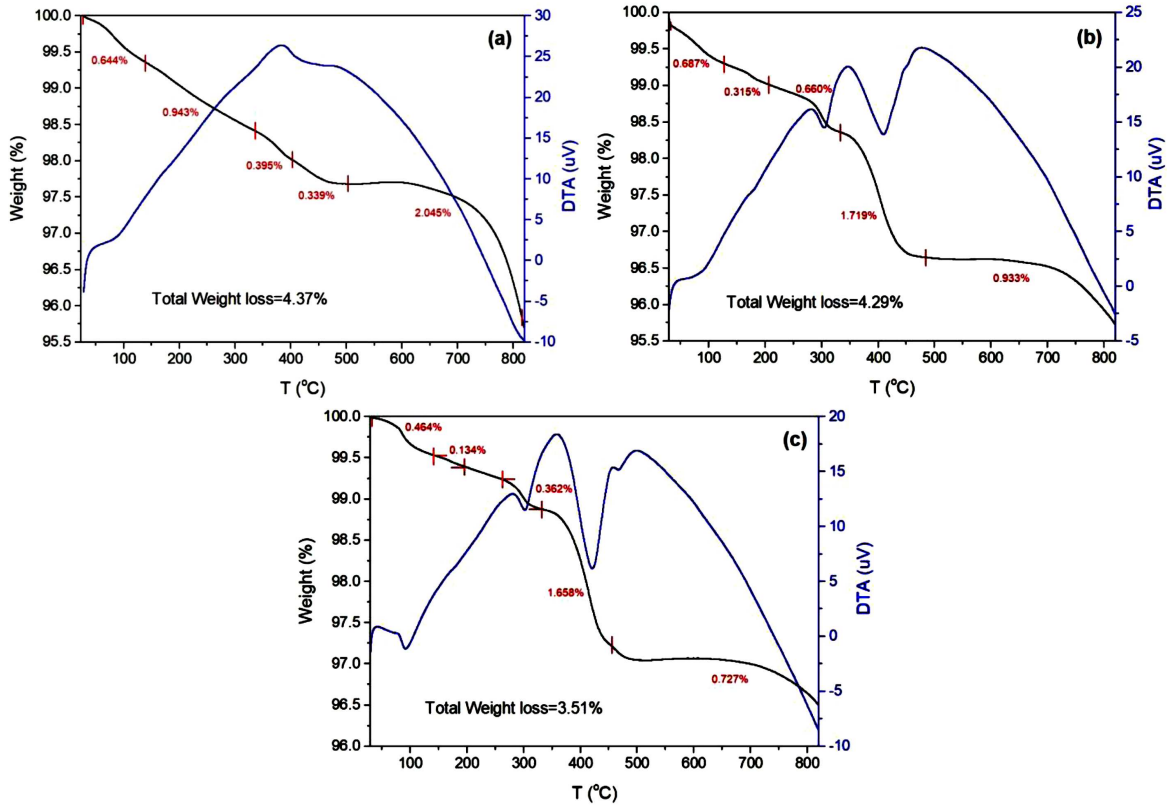

Figure 5. TG/DTA curves of the powders (heated at 950 °C): a) $BiSr_2CaCu_2O_{6.5}$, b) $Eu_{0.3}Bi_{0.7}Sr_2CaCu_3O_{6.5}$ and c) $Eu_{0.5}Bi_{0.5}Sr_2CaCu_3O_{6.5}$

increase in the height of the peak confirmed the increasing Eu substitution in the samples. The chemical compositions of the samples were also given in Table 1.

The SEM micrographs of the sintered samples were shown in Fig. 4. Homogenous morphology and almost equal grain size distribution were observed for $BiSr_2CaCu_2O_{6.5}$. As the europium substitution increases in the material, the grain size distribution becomes inhomogeneous. Additionally, the well-faceted grain boundaries can be seen in Fig. 4. The insets in Fig. 4 also show the SEM micrographs of the powder samples. All samples have a layered structure which is made up of plates with different shapes whose average size is between 1–5 μm. $BiSr_2CaCu_2O_{6.5}$

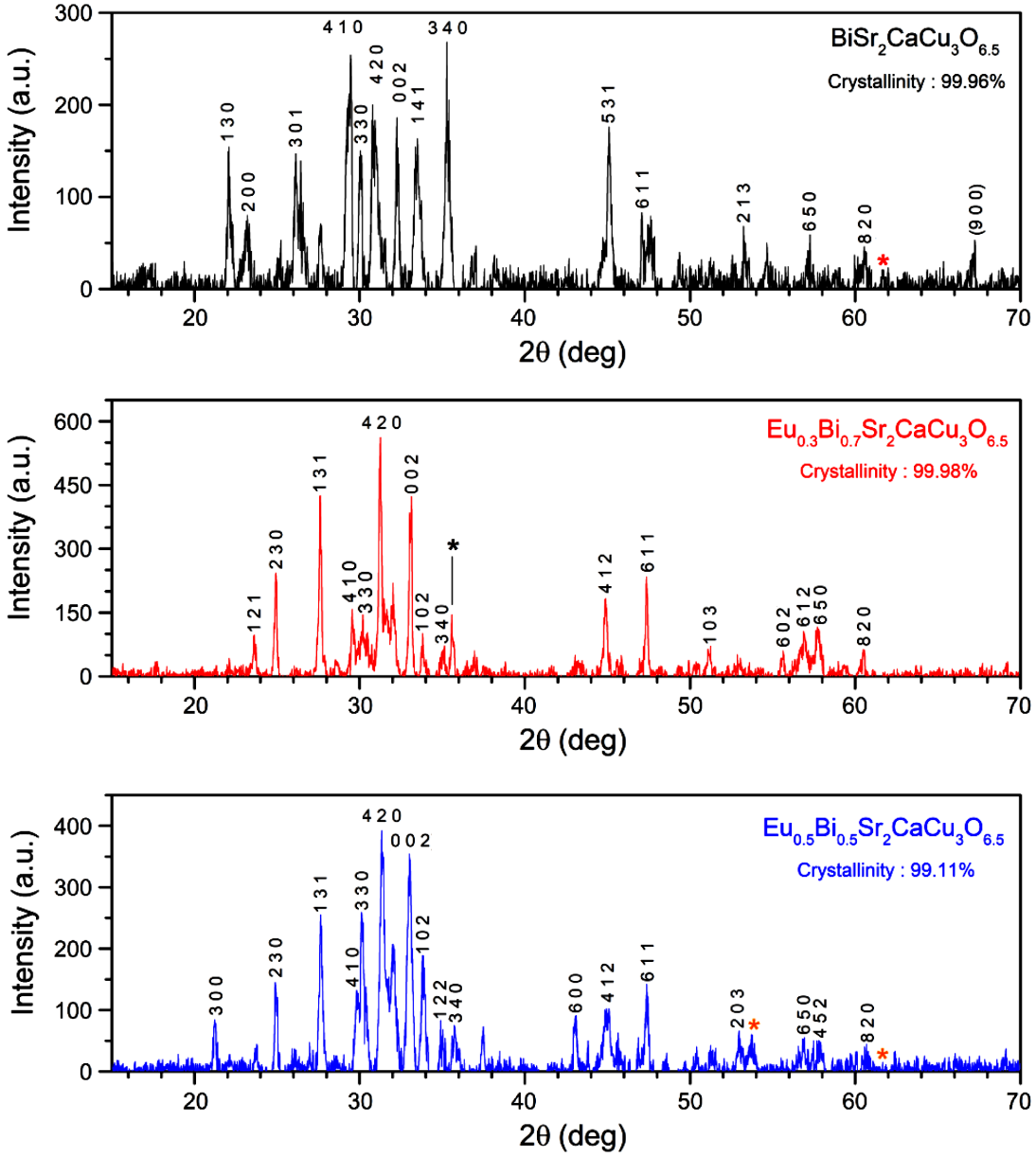

Figure 6. XRD patterns of the powders (heated at 950 °C): a) $BiSr_2CaCu_2O_{6.5}$, b) $Eu_{0.3}Bi_{0.7}Sr_2CaCu_3O_{6.5}$ and c) $Eu_{0.5}Bi_{0.5}Sr_2CaCu_3O_{6.5}$

also shows the mica-like ceramic structure which is consistent with the mica-like layered building blocks structure characteristic for bismuth-containing ceramics [15]. The well-faceted grain boundaries can be seen in Fig. 4. Moreover, as shown in Fig. 4c, europium substitution in the pure $BiSr_2CaCu_2O_{6.5}$ system causes a pentagonal shaped layered structure. The mass densities of the $BiSr_2CaCu_2O_{6.5}$, $Eu_{0.3}Bi_{0.7}Sr_2CaCu_3O_{6.5}$ and $Eu_{0.5}Bi_{0.5}Sr_2CaCu_3O_{6.5}$ samples were determined as 4.96, 3.95 and 3.90 g/cm^3, respectively.

The total weight losses of the samples after the heating process up to 820 °C were given in Fig. 5. According to TG analysis, as the amount of Eu increases in the material, the total weight loss decreases from 4.37% to 3.51%. In this context, Eu substitution increased the thermal stability of the Bi-Sr-Ca-Cu-O in the related temperature interval. On the other hand, while one step pattern of thermal degradation was observed for the $BiSr_2CaCu_2O_{6.5}$ sample, two-steps pattern was determined for the Eu substituted $BiSr_2CaCu_2O_{6.5}$.

The XRD patterns and the Miller indices of the crystal planes' reflections were shown in Fig. 6. Additionally, an impurity phase associated with CuO has been indexed by star symbol in the XRD patterns. As shown in Fig. 6, similar to other Bi-based phases such as $(Bi,Pb)Sr_2(Y,Ca)Cu_2O_{7-z}$ [16] and $(Tl,Bi)Sr_2(Ca,Y)Cu_2O_7$ [17], it was found that $BiSr_2CaCu_2O_{6.5}$ and the Eu-substituted samples crystallize in tetragonal structure. Additionally, the diffraction peaks shifted towards higher 2θ angles with increasing Eu substitution. The similar peak shift was also reported for the Eu substituted $Bi_{1.6}Pb_{0.5}Sr_{2-x}Eu_xCa_{1.1}Cu_{2.1}O_y$ (where $0 \leq x \leq 0.5$) [18] and $Ba_6(Bi_{1-x}Eu_x)_9B_{79}O_{138}$ (where $0 \leq x \leq 1$) [19] materials.

3.2. Dielectric properties

The complex dielectric function ε^* is defined by:

$$\varepsilon^* = \varepsilon' - j\varepsilon'' \quad (1)$$

where ε' and ε'' are the real and imaginary components of the complex dielectric function, respectively. While the real part of ε^* represents the charge storage ability of the dielectric material, the imaginary component of ε^* determines the dielectric loss.

The frequency dependencies of the real and imaginary parts of the complex dielectric function of the samples at room temperature were given in Figs. 7a and 7b, respectively. As shown in Fig. 7a, ε' value increased with increasing heavy rare earth element (i.e. Eu) concentration. On the other hand, dielectric loss (ε'') value decreased considerably with increasing europium content in the material (Fig. 7b). It was determined that while the real part of the complex dielectric function is increased 3.8 times for $x = 0.5$ Eu substitution, dielectric loss is decreased 32 times at room temperature. From this point of view, the highest charge storage ability with the lowest dielectric loss at room temperature was obtained for $Eu_{0.5}Bi_{0.5}Sr_2CaCu_3O_{6.5}$ ceramics. In this context, it was suggested that $Eu_{0.5}Bi_{0.5}Sr_2CaCu_3O_{6.5}$ ceramics may be used as a good insulating material for capacitor applications.

ε'' versus frequency curves of the samples given in Fig. 7b showed similar behaviour with increasing frequency. The most important feature of the material is the decrease of the dielectric loss by 100 times with substituting europium in the $BiSr_2CaCu_2O_{6.5}$ system. According to Feng *et al.* [23] the decrease in the dielectric loss in "ILBC dielectric material" can be associated with the increase of conductivity in the (Eu/Bi)-Sr-Ca-Cu-O grain/subgrain. In this context, europium substitution achieved to increase the resistivity of the insulating barriers in the materials which leads to the increase of grain boundary resistance at low frequency. This prediction was also confirmed by complex impedance measurements.

3.3. Electrical modulus properties

To distinguish localized dielectric relaxation process from long range conductivity, complex dielectric and electrical modulus graphics of the samples were also compared.

As it is known, complex electrical modulus, M^*, is defined as:

$$M^* = M' - jM'' = (\varepsilon^*)^{-1} \quad (2)$$

The frequency dependences of the real and imaginary components of the complex electrical modulus of the

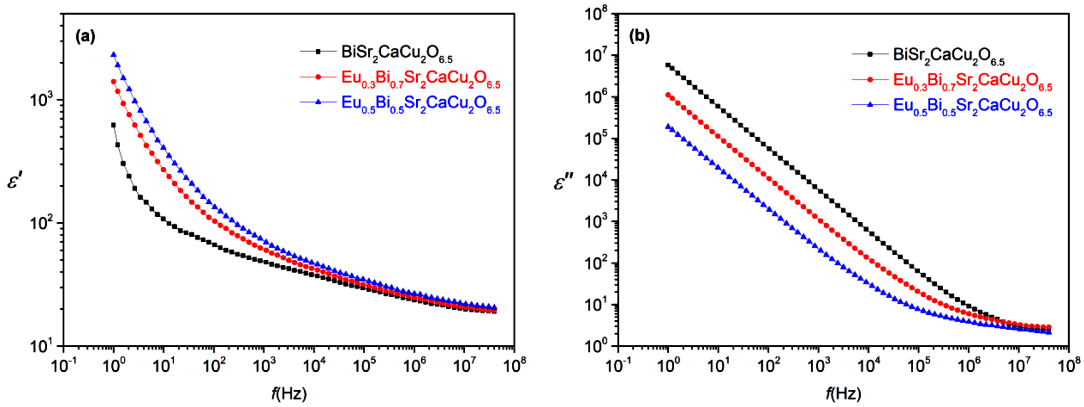

Figure 7. The frequency dependence of: a) the real and b) imaginary components of the complex dielectric function of the samples at room temperature

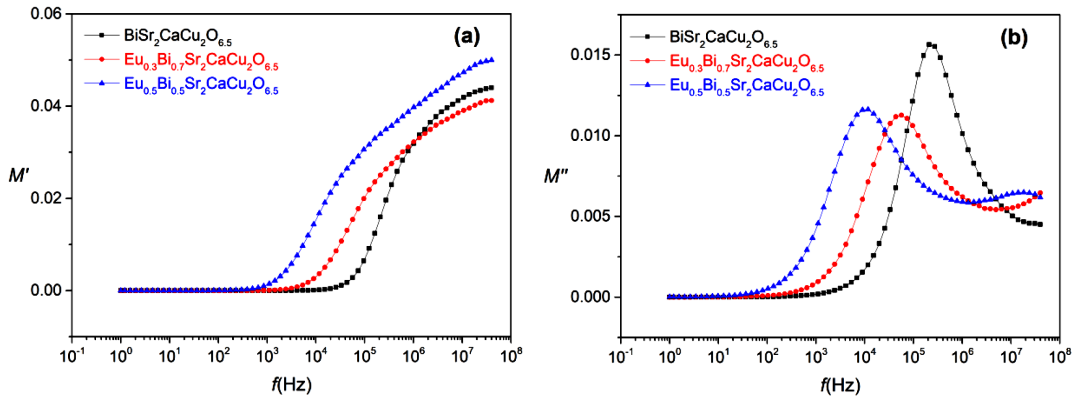

Figure 8. The frequency dependence of: a) the real and b) imaginary components of complex electrical modulus of the samples at room temperature

samples are given in Fig. 8a and 8b, respectively. The frequency dependences of the real part of the complex electrical modulus of the samples displayed frequency independent behaviour from low frequencies to mid-frequencies with zero value and showed increasing behaviour at high frequencies. Approximately zero value of M' at low frequencies also verified the removal of electrode polarization effect and indicated the conduction phenomena due to the long-range mobility of charge carriers in the material [26,27].

On the other hand, M'' showed frequency independent plateau for the low frequencies, then increased with the increase of frequency, displayed a peak and finally it decreased with frequency. In addition, the asymmetric modulus peak appearing in M'' versus frequency curve shifted towards the lower frequencies with increasing europium substitution. The shift of modulus peak to the lower frequencies due to the increased europium substitution represented the range of frequencies in which the ions are capable of moving at long distances by performing hopping from one site to the neighbouring ones [28,29]. In addition, pure conduction process manifests itself as an occurrence of a peak only in $M'' = f(\omega)$ spectra. On the other hand, localized dielectric relaxation process is characterized by the appearance of peaks in both $\varepsilon'' = f(\omega)$ and $M'' = f(\omega)$ spectra [30–32]. In this context, the comparison of Figs. 7b and 8b revealed that the samples exhibited pure conduction process.

In general, the Cole-Cole plot in complex electrical modulus plane is more effective for determining the contribution from grains and grain boundaries. Due to this reason, the Cole-Cole plots in complex electrical modulus plane of the samples have also been investigated (Fig. 9). As it is seen, the complex electric modulus spectra of the samples did not constitute a complete semicircle. Instead of complete semicircles, the samples displayed deformed arcs whose centres were positioned below the real axis. This behaviour of the Cole-Cole plots also indicated the non-Debye type of relaxation process. Moreover, while pure $BiSr_2CaCu_2O_{6.5}$ displayed strong grain effect due to the observation of approximately single deformed semicircle, europium substituted $BiSr_2CaCu_2O_{6.5}$ samples displayed both grain and grain boundary effects at the high and low frequencies, respectively.

The temperature dependence of M'' versus frequency curves were given in Figs. 10a, 10b and 10c for the $BiSr_2CaCu_2O_{6.5}$, $Eu_{0.3}Bi_{0.7}Sr_2CaCu_3O_{6.5}$ and $Eu_{0.5}Bi_{0.5}Sr_2CaCu_3O_{6.5}$, respectively. It was clearly observed that M'' peak shifts to the high-frequency region with increasing temperature from 293 K to 433 K for all samples. This characteristic behaviour of M'' versus frequency curves implied the temperature-activated relaxation process which can be attributed to the Maxwell-Wagner type polarization effect. The Maxwell-Wagner type polarization of the samples was also suggested in the dielectric results section. It indicates that the grain boundaries have a crucial influence on the dielectric properties of the material investigated [33,34].

Temperature dependence of the relaxation time (τ) was investigated by determining relaxation frequencies (f_r) at which the maximum M'' is observed. Relaxation time was calculated by the relation $\tau = 1/2\pi f_r$. The activation energies of the samples were calculated from the slope of the Arrhenius plot of relaxation time given in Fig. 10d.

The Arrhenius equation is described by:

$$\tau = \tau_0 \cdot \exp\left(\frac{E_a}{k_B T}\right) \tag{3}$$

where E_a represents the activation energy, τ_0 is the mean relaxation time and k_B is the Boltzmann constant. As shown in Fig. 10d, activation energy increased with increasing Eu substitution. The increase in activation energy can be attributed to the fact that the conduction process is getting harder by Eu substitution which results in obtaining better insulating material with a higher ε' value.

3.4. Impedance spectra of the samples

In Fig. 11, the frequency dependences of the real and imaginary component of the impedance together with the Cole-Cole plots were shown.

$Z' = f(\omega)$ curves of the samples exhibited three different behaviours with increasing frequency (Fig. 11a): approximately frequency independent plateau, decreasing Z' with increasing frequency and approach to the lowest value of Z' at high-frequency region. The decrease of Z' values with increasing frequency can be interpreted as an enhancement of the mobility of charge

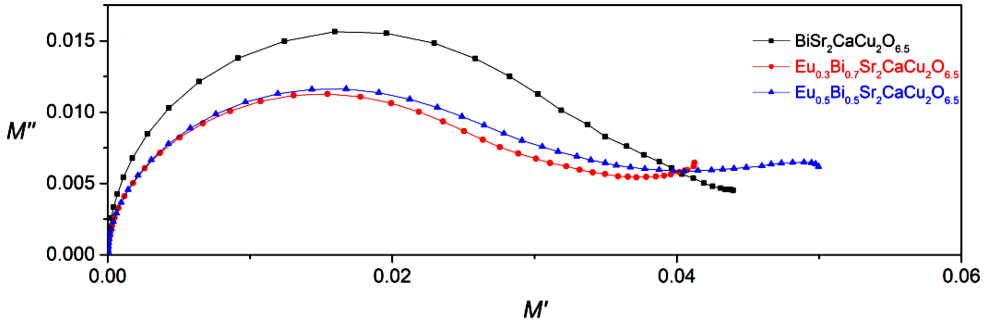

Figure 9. The Cole-Cole plots in complex electrical modulus plane for the samples

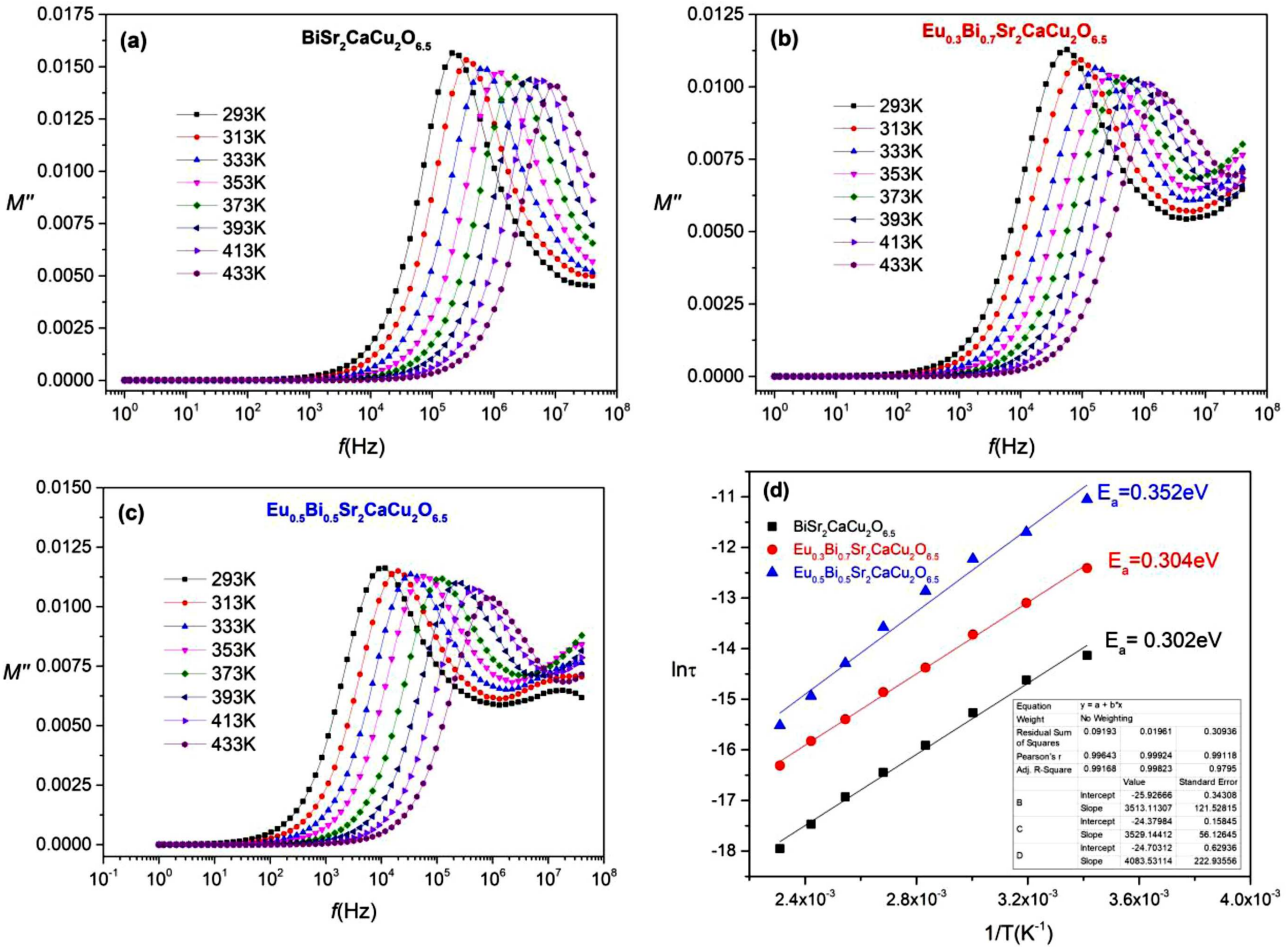

Figure 10. The temperature dependent M'' versus frequency curves for: a) $BiSr_2CaCu_2O_{6.5}$, b) $Eu_{0.3}Bi_{0.7}Sr_2CaCu_3O_{6.5}$, c) $Eu_{0.5}Bi_{0.5}Sr_2CaCu_3O_{6.5}$ and d) Arrhenius plot of the relaxation time

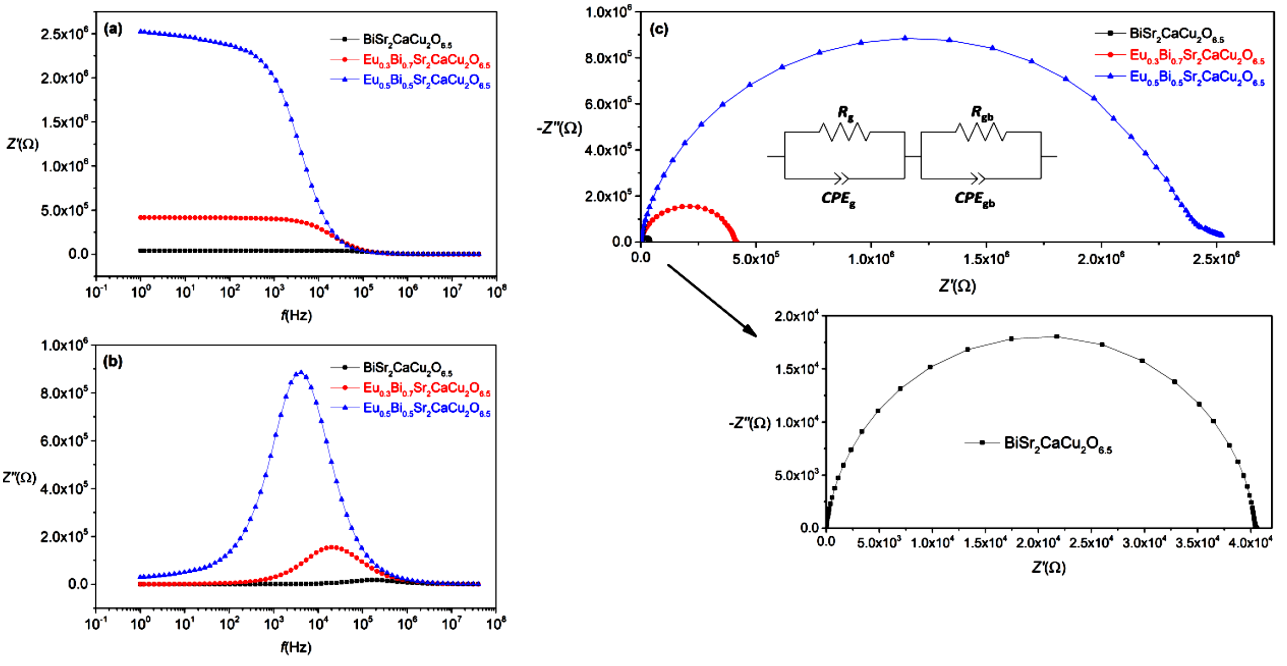

Figure 11. The frequency dependence of: a) the real and b) imaginary components of the impedance function at room temperature, and c) the Cole-Cole plots of the samples

Table 2. Equivalent circuit fitting parameters of the impedance

	$BiSr_2CaCu_2O_{6.5}$	$Eu_{0.3}Bi_{0.7}Sr_2CaCu_3O_{6.5}$	$Eu_{0.5}Bi_{0.5}Sr_2CaCu_3O_{6.5}$
R_g [Ω]	2.518×10^4	2.605×10^5	1.622×10^6
R_{gb} [Ω]	4.065×10^4	4.164×10^5	2.441×10^6
CPE_g	2.179×10^{-11}	1.527×10^{-11}	1.412×10^{-11}
CPE_{gb}	3.434×10^{-11}	3.266×10^{-11}	2.508×10^{-11}

carriers. In addition, merging of the same Z' values at high frequency for all samples indicated the existence of space charge polarization in the material [35]. On the other hand, it was determined that Z' values at low and mid-frequency region considerably increases with europium substitution. This means that Eu substitution increases grain boundary resistance which results in the increase of the real part complex dielectric function. The similar results were reported for $CaTiO_3$ and ZrO_2 doping in $CaCuTiO_{14}$ ceramics [36,37].

As shown in Fig. 11b, the absolute value of the imaginary component of complex impedance function of all samples showed an increasing behaviour with increasing frequency up to the certain frequency, then started to decrease and reached its minimum value. The critical frequency at which maximum Z'' is observed shifted from 164.14 kHz to 4.06 kHz with increasing europium substitution in $BiSr_2CaCu_2O_{6.5}$.

The Cole-Cole plots, shown in Fig. 11c, have a depressed semicircular arc which can be fitted by considering both the grain and grain boundary contributions. The depressed semicircle also implies the non-Debye type of relaxation in the samples. While the low and mid-frequency arcs correspond to the grain boundary effect, the high-frequency one is due to the grain contribution. As it is illustrated in Fig. 11c, the equivalent circuit of the samples can be modelled by considering both contributions with a serial combination of two parallel combinations of a resistor and constant phase element (*CPE*). In our situation, the curves were fitted with parallel resistances (R) and constant phase elements (*CPE*s) instead of parallelly connected R and C elements since *CPE* is used to evaluate the Non-Debye type relaxation. In the equivalent circuit, one parallelly connected R and *CPE* pair corresponds to the grain effect, the other one represents the grain boundary effect. The related equivalent circuit parameters were given in Table 2. The presented data confirmed that the grain boundaries are more resistive and capacitive than the grains for each sample. On the other hand, it was also determined that as the Eu substitution increases, R_g and R_{gb} values increase while C_g and C_{gb} values decrease.

IV. Conclusions

In this work, europium substituted $BiSr_2CaCu_2O_{6.5}$ ceramic samples were synthesized for the first time. The pure and europium substituted $BiSr_2CaCu_2O_{6.5}$ samples, sintered at 950 °C for 24 h, were characterized in terms of their chemical compositions, microstructures and morphologies. Dielectric properties were investigated between 1 Hz and 40 MHz varying from room temperature to 433 K. Dielectric measurements revealed that $Eu_{0.5}Bi_{0.5}Sr_2CaCu_3O_{6.5}$ sample exhibits a higher dielectric constant and lower dielectric loss relative to $BiSr_2CaCu_2O_{6.5}$. In this context, partial europium substitution into $BiSr_2CaCu_2O_{6.5}$ system was suggested as an effective dopant for obtaining better dielectric material with the lower dielectric loss. The results have also been confirmed by analysis of the temperature dependent complex electrical modulus of the samples. The temperature dependence of the relaxation time analysis pointed out that partially europium substitution increased the activation energies which resulted in a harder conduction process in the material that causes to obtain a high dielectric constant material. Ultimately, $Eu_{0.5}Bi_{0.5}Sr_2CaCu_3O_{6.5}$ material may have a promising potential for capacitor applications which require high dielectric constant with the low dielectric loss.

Acknowledgement: This research has been supported by Yildiz Technical University Scientific Research Projects Coordination Department with the Project Number 2014-01-01-GEP04.

References

1. S.K. Gupta, J. Singh, J. Akhtar, "Materials and processing for gate dielectrics on silicon carbide (SiC) surface", pp. 208–234 in *Physics and Technology of Silicon Carbide Devices*. Ed. by Y. Hijikata, InTech, Croatia, 2013.
2. J. Reynard, C. Verove, E. Sabouret, P. Motte, B. Descouts, C. Chaton, J. Michailos, K. Barla, "Integration of fluorine-doped silicon oxide in copper pilot line for 0.12-μm technology", *Microelectron. Eng.*, **60** (2002) 113–118.
3. J. Robertson, "High dielectric constant oxides", *Eur. Phys. J. Appl. Phys.*, **28** (2004) 265–291.
4. A. Istratov, E. Weber, "Physicochemical properties of selected 4d, 5d, and rare earth metals in silicon", pp. 359–378 in *High Dielectric Constant Materials*. Eds. by H.R. Huff, D.C. Gilmer, Springer, Germany, 2005.
5. J.M. Tarascon, W.R. McKinnon, P. Barboux, D. Hwang, B.G. Bagley, L.H. Greene, G.W. Hull, Y. LePage, N. Stoffel, M. Giroud, "Preparation, structure, and properties of the superconducting compound series $Bi_2Sr_2Ca_{n-1}Cu_nO_y$ with n = 1, 2, and 3", *Phys. Rev. B.*, **38** (1988) 8885–8892.
6. F. Granados-Correa, J. Bonifacio-Martínez, "Combustion synthesis process for the rapid preparation of high-purity SrO powders", *Mater. Sci-Poland*, **32** (2014) 682–687.
7. Y. Hu, N.-H. Liu, U.-L. Lin, "Glass formation and glass structure of the $BiO_{1.5}$-PbO-CuO system", *J. Mater. Sci.*, **33** (1998) 229–234.
8. R. Bala, A. Agarwal, S. Sanghi, S. Khasa, "Influence of SiO_2 on the structural and dielectric properties of $ZnO \cdot Bi_2O_3 \cdot SiO_2$ glasses", *J. Integr. Sci. Technol.*, **3**

(2015) 6–13.
9. K. Ghanbari, Z. Babaei, "Fabrication and characterization of non-enzymatic glucose sensor based on ternary NiO/CuO/polyaniline nanocomposite", *Anal. Biochem.*, **498** (2016) 37–46.
10. R. Choudhary, S. Koppala, S. Swamiappan, "Bioactivity studies of calcium magnesium silicate prepared from eggshell waste by sol-gel combustion synthesis", *J. Asian Ceram. Soc.*, **3** (2015) 173–177.
11. F. Cui, T. Cui, "Self-catalytic synthesis of metal oxide nanoclusters@mesoporous silica composites based on successive spontaneous reactions at near neutral conditions", *Chem. Commun.*, **50** (2014) 14801–14804.
12. R. Iordanova, V. Dimitrov, Y. Dimitriev, D. Klissurski, "Glass formation and structure of glasses in the V_2O_5-MoO_3-Bi_2O_3system", *J. Non-Cryst. Solids*, **180** (1994) 58–65.
13. P. Pascuta, G. Borodi, E. Culea, "Influence of europium ions on structure and crystallization properties of bismuth borate glasses and glass ceramics", *J. Non-Cryst. Solids*, **354** (2008) 5475–5479.
14. P. Pascuta, G. Borodi, E. Culea, "Structural investigation of bismuth borate glass ceramics containing gadolinium ions by X-ray diffraction and FTIR spectroscopy", *J. Mater. Sci.: Mater. Electron.*, **20** (2009) 360–365.
15. V. Fruth, M. Popa, A. Ianculescu, M. Stir, S. Preda, G. Aldica, "High-Tc phase obtained in the Pb/Sb doped Bi-Sr-Ca-Cu-O system", *J. Eur. Ceram. Soc.*, **24** (2004) 1827–1830.
16. H. Frank, R. Stollmann, J. Lethen, R. Müller, L. Gasparov, N. Zakharov, D. Hesse, G. Güntherodt, "Preparation and magnetic properties of (Bi, Pb)-1212", *Physica C*, **268** (1996) 100–106.
17. A.A. Yusuf, A. Yahya, F.M. Salleh, "Formation and characterization of (Tl, M) Sr1212 (M = Bi, Pb, Cr) Superconducting ceramics", *Malaysian J. Analyt. Sci.*, **16** (2012) 12–17.
18. S. Vinu, P. Sarun, A. Biju, R. Shabna, P. Guruswamy, U. Syamaprasad, "The effect of substitution of Eu on the critical current density and flux pinning properties of (Bi, Pb)-2212 superconductor", *Supercond. Sci. Tech.*, **21** (2008) 045001.
19. Q. Li, R. Cong, X. Zhou, W. Gao, T. Yang, "$Ba_6(Bi_{1-x}Eu_x)_9B_{79}O_{138}$ ($0 \leq x \leq 1$): synergetic changing of the wavelength of Bi^{3+} absorption and the red-to-orange emission ratio of Eu^{3+}", *J. Mater. Chem. C*, **3** (2015) 6836–6843.
20. C. Koops, "On the dispersion of resistivity and dielectric constant of some semiconductors at audiofrequencies", *Phys. Rev.*, **83** (1951) 121–124.
21. J. Maxwell, *Electricity and Magnetism*, Clarendon Press, Oxford, 1873.
22. K.W. Wagner, "Zur theorie der unvollkommenen dielektrika", *Ann. Phys-Berlin*, **345** (1913) 817–855.
23. L. Feng, X. Tang, Y. Yan, X. Chen, Z. Jiao, G. Cao, "Decrease of dielectric loss in $CaCu_3Ti_4O_{12}$ ceramics by La doping", *Phys. Status Solidi A*, **203** (2006) R22–R24.
24. D.C. Sinclair, T.B. Adams, F.D. Morrison, A.R. West, "$CaCu_3Ti_4O_{12}$: one-step internal barrier layer capacitor", *Appl. Phys. Lett.*, **80** (2002) 2153–2155.
25. S. Sarkar, P.K. Jana, B. Chaudhuri, "Colossal internal barrier layer capacitance effect in polycrystalline copper (II) oxide", *Appl. Phys. Lett.*, **92** (2008) 022905.
26. B. Chowdari, R. Gopalakrishnan, "AC conductivity analysis of glassy silver iodomolybdate system", *Solid State Ionics*, **23** (1987) 225–233.
27. C.V.S. Reddy, X. Han, Q.-Y. Zhu, L.-Q. Mai, W. Chen, "Dielectric spectroscopy studies on (PVP + PVA) polyblend film", *Microelectron. Eng.*, **83** (2006) 281–285.
28. J.S. Kim, "Electric modulus spectroscopy of lithium tetraborate ($Li_2B_4O_7$) single crystal", *J. Phys. Soc. Jpn.*, **70** (2001) 3129–3133.
29. Q. Li, H. Wang, H. Fan, M. Xu, B. Peng, C. Long, X. Liu, "Dielectric properties and electrical conduction of La_2O_3-doped $(Bi_{0.5}Na_{0.5})_{0.94}Ba_{0.06}TiO_3$ ceramics", *Appl. Phys. A*, **114** (2014) 551–558.
30. R. Gerhardt, "Impedance and dielectric spectroscopy revisited: distinguishing localized relaxation from long-range conductivity", *J. Phys. Chem. Solids*, **55** (1994) 1491–1506.
31. I. Hodge, M. Ingram, A. West, "Impedance and modulus spectroscopy of polycrystalline solid electrolytes", *J. Electroanal. Chem. Interfacial Electrochem.*, **74** (1976) 125–143.
32. J. Liu, C.-G. Duan, W.-G. Yin, W.-N. Mei, R.W. Smith, J.R. Hardy, "Dielectric permittivity and electric modulus in $Bi_2Ti_4O_{11}$", *J. Chem. Phys.*, **119** (2003) 2812–2819.
33. J. Liu, C.-g. Duan, W.-N. Mei, R.W. Smith, J.R. Hardy, "Dielectric properties and Maxwell-Wagner relaxation of compounds $ACu_3Ti_4O_{12}$ (A = Ca, $Bi_{2/3}$, $Y_{2/3}$, $La_{2/3}$)", *J. Appl. Phys.*, **98** (2005) 093703.
34. J. Liu, C.-G. Duan, W.-G. Yin, W.-N. Mei, R.W. Smith, J.R. Hardy, "Large dielectric constant and Maxwell-Wagner relaxation in $Bi_{2/3}Cu_3Ti_4O_{12}$", *Phys. Rev. B*, **70** (2004) 144106.
35. H. Rahmouni, M. Smari, B. Cherif, E. Dhahri, K. Khirouni, "Conduction mechanism, impedance spectroscopic investigation and dielectric behavior of $La_{0.5}Ca_{0.5-x}Ag_xMnO_3$ manganites with compositions below the concentration limit of silver solubility in perovskites ($0 \leq x \leq 0.2$)", *Dalton Trans.*, **44** (2015) 10457–10466.
36. W. Kobayashi, I. Terasaki, "$CaCu_3Ti_4O_{12}$/$CaTiO_3$ composite dielectrics: Ba/Pb-free dielectric ceramics with high dielectric constants", *App. Phys. Lett.*, **87** (2005) 032902.
37. E.A. Patterson, S. Kwon, C.-C. Huang, D.P. Cann, "Effects of ZrO_2 additions on the dielectric properties of $CaCu_3Ti_4O_{12}$", *App. Phys. Lett.*, **87** (2005) 182911.